In Situ Studies of Ion Irradiation Effects in an Electron Microscope

J.S. VETRANO, M.W. BENCH, I.M. ROBERTSON, and M.A. KIRK

The High-Voltage Electron Microscope (HVEM)-Accelerator Facility at Argonne National Laboratory (ANL) has been used to gain insight into the process of collapse of displacement cascades to vacancy loops in metals (Ni, Cu, Fe, Ni-Si, and Ni-Al) and the crystalline-amorphous transition produced in GaAs by ion implantation.

I. INTRODUCTION

THE HVEM-Accelerator Facility at ANL is comprised of an AEI EM-7, 1.2 MeV electron microscope and two ion accelerators, a 650 keV NEC and a 2 MeV NEC Tandem accelerator.[1,2] The beams from either accelerator can be directed, through an ion-beam interface, into the specimen chamber of the HVEM. Microscope sample stages allow the sample temperature to be varied from 10 to 1000 K; the sample resistivity can also be monitored in the low-temperature stages. This coupling of an ion accelerator to an electron microscope affords the experimentalist a unique opportunity to perform heavy-ion irradiations and electron microscopy at the same temperature within the same instrument. This permits direct observation of effects such as the buildup of the defect structure as the ion dose is increased; the fate of individual defects as the ion dose is increased; the effect of varying the mobility of the point defects (sample temperature); and irradiation-induced transformations. The potential of this facility will be demonstrated by means of examples. The first example compares the buildup of defects with increasing ion dose at 30 and 300 K in different metals (Cu, Fe, Ni, and dilute Ni alloys). The second considers aspects of the crystalline-amorphous transition induced in the compound semiconductor, GaAs, by ion implantation and the subsequent recrystallization of the amorphous zones.

II. EXPERIMENTAL PROCEDURES

The samples were irradiated as thinned 3-mm transmission electron microscope (TEM) discs. The metal discs were taken from high-purity stock material, vacuum annealed, and then jet electropolished to perforation by using standard solutions.[3] The GaAs, which was obtained from the Morgan Semiconductor Company, Garland, TX, was first mechanically dimpled and then perforated using a chemical polish of sulfuric acid, hydrogen peroxide, and water in a ratio of 4:1:1. Considerable care was taken during sample preparation to ensure that the sample surfaces were free from artifacts that could be mistaken for radiation-induced defects. Surface deterioration was minimized by storing the samples under vacuum prior to and after the irradiation experiments.

The samples were irradiated with 50 and 100 keV ions (Ni^+, Fe^+, Cu^+, Ar^+, Kr^+, and Xe^+). The ion dose rate was typically 10^{10} ions cm^{-2} s^{-1}, and the ion dose was in the range of 10^{11} to 5×10^{13} ions cm^{-2}. Low ion doses were used to avoid the complication of having spatially overlapping displacement cascades: significant spatial overlap occurs at ion doses exceeding 1×10^{12} ions cm^{-2}.

The irradiations and the electron microscopy were performed at 300 and 30 K. Comparison of the defect structures produced at these two irradiation temperatures and the structural changes occurring upon warming from 30 K to room temperature allows us to elucidate the mechanisms of defect formation from displacement cascades. Low temperatures (30 K) were achieved by flowing helium, either in a liquid or a gas phase, through the rear of the sample rod. The flowing coolant and oscillations of the liquid in the reservoir produced high- and low-frequency sample oscillations. The high-frequency oscillations impose a limit on these experiments, restricting the size of the defect that can be observed to above a diameter of about 1.5 nm. This value may vary from sample to sample, due to the variation in the quality of the sample. The low-frequency sample oscillations make image recording difficult. This was usually overcome by using short exposure times (0.5 or 1 second). High-quality images were obtained with these short exposure times by using a high-speed film, KODAK* 645, which has a speed six times faster than the more conventional microscope film SO 163. (KODAK 645 has to be specially ordered from the manufacturer). Additional follow-up microscopy was performed in a PHILIPS** EM 420, 430, or CM30.

During irradiations, the ion dosimetry is monitored by measuring the current in an annular Faraday cup positioned about 10 cm from the sample. The accuracy of measuring the ion dosimetry by this technique can be checked by irradiating, to low ion doses, an ordered alloy (*e.g.*, Ni_3Al) in which every incident ion creates a disordered zone. The disordered zones are rendered visible

J.S. VETRANO and M.W. BENCH, Graduate Students, and I.M. ROBERTSON, Associate Professor, are with the Department of Materials Science and Engineering, University of Illinois, Urbana, IL 61801. M.A. KIRK, Metallurgist, is with the Materials Science Division, Argonne National Laboratory, 9700 S. Cass Avenue, Argonne, IL 60439.

This paper is based on a presentation made in the symposium "Irradiation-Enhanced Materials Science and Engineering" presented as part of the ASM INTERNATIONAL 75th Anniversary celebration at the 1988 World Materials Congress in Chicago, IL, September 25–29, 1988, under the auspices of the Nuclear Materials Committee of TMS-AIME and ASM-MSD.

*KODAK is a trademark of Eastman Kodak Corporation, Rochester, NY.

**PHILIPS is a trademark of Philips Instruments Corporation, Mahwah, NJ.

in the electron microscope by imaging with a superlattice reflection, and the ion dose is determined by counting the number of disordered zones in a known area. Thus, the Faraday cup measurement of the ion dose is determined to be accurate to ±10 pct; that is, for this work, the annular Faraday cup has an absolute accuracy of 1×10^{10} ions cm^{-2}.

The defects produced in the metals were imaged under dynamical two-beam, dark-field conditions with the low-order reflections found around major zones. The Burgers vectors of the loops were determined by using the $\mathbf{g} \cdot \mathbf{b} = 0$ invisibility condition and by matching the changes in the image symmetry for different reflections with those predicted by computer simulations (see Reference 4 for fcc systems and References 5 and 6 for bcc systems). For a black-white lobe image, the size of the defect is the length of the interface separating the lobes, and for a black dot image, it is the maximum dimension. Saldin *et al.*[4] have shown that these dimensions approximately correspond to the size of the actual defect. The defect yield, which is defined as the number of visible defects per incident ion, is determined from dark-field images taken in the (200) reflection. In fcc systems, the majority of loops are imaged with this single reflection; only one-third of the perfect loops (Burgers vector = $\mathbf{a}/2\langle 110\rangle$) are omitted. In bcc systems, a (200)-type reflection will image all loops with a Burgers vector of the $\mathbf{a}/2\langle 111\rangle$ type and one-third of the loops with an $\mathbf{a}\langle 100\rangle$ Burgers vector.

In the compound semiconductor GaAs, the defects produced by ion implantation are imaged using the fundamental reflections (220) and (400) and the superlattice reflection (200). The fundamental reflection is sensitive to lattice strains and differences in the amorphous and crystalline material, whereas the superlattice reflection is additionally sensitive to antisite disorder.

III. RESULTS AND DISCUSSION

A. *Case 1: The Formation of Vacancy Loops in Metals from Heavy-Ion Generated Displacement Cascades*

The defect structure of a displacement cascade, as determined by computer simulation techniques, consists of a vacancy-rich region with the interstitials dispersed around the periphery.[7,8] Recent molecular dynamic computer simulations[8] have shown that as a consequence of the amount of energy deposited in the core region, the atoms are extremely agitated and are in a state analogous to that in a liquid. The resolidification occurs from the outer edge, and since the fluctuations in the atomic density are least at the periphery of the cascade zone, few vacancies are retained in this region. As regrowth continues, the density fluctuations increase due to the missing atoms, and vacancies are grown in the solid. This results in the vacancies concentrating in the cascade center, a condition that favors loop formation.

Comparison of the computer simulations of the displacement cascades generated in Ni and Cu have shown that they are similar: both have molten zones, and the decrease in the atomic density in the cascade core region is about 15 pct, but the disorder lasts longer in Cu than in Ni.[9] For example, 3.7 picoseconds after the cascade is created, the molten zone in Ni has completely recrystallized, whereas in Cu, it has shrunk but is still disordered.[9] Because of the shorter molten zone lifetime in Ni, there is less time for atomic rearrangement, and the vacancies will be distributed throughout the cascade volume. Thus, the condition of a high-vacancy concentration which would favor loop formation is less likely to be attained in Ni than in Cu. Experiments show that cascade collapse to a vacancy loop is more probable in Cu than in Ni.

This material difference is rather surprising, as the elements are similar in mass and have the same structure, which would suggest that the dynamics of the cascade should be rather similar. The primary difference between Ni and Cu is the melting temperature, being 1726 and 1356 K, respectively. Flynn and Averback[10] have suggested that the difference in the loop formation probabilities in Cu and Ni may not be entirely due to the differences in the material melting temperature but may also reflect differences in the coupling between the electron and phonon systems. Strong electron-phonon coupling would cause the thermal spike to quench faster, because the heat capacity of the electrons will absorb energy and the high thermal conductivity of the electrons will rapidly dissipate the energy. Since the density of states near the Fermi level is ten times higher in Ni than in Cu, the molten zone lifetime may be shorter in Ni than in Cu.

The computer simulations have provided a possible explanation for the formation of a vacancy loop from a displacement cascade but have not themselves shown cascade collapse. Attempts at simulating this event have had to assume unrealistic starting configurations.[11,12,13]

Vacancy loops, because of their strain field, are amenable to investigation by transmission electron microscopy. The Argonne HVEM-Accelerator Facility has been used to investigate the probability of a displacement cascade collapsing to a vacancy loop in a number of materials, Fe,[14] Ni,[15] Ag,[16] and Cu_3Au,[17] as a function of irradiation temperature and ion dose. The Argonne Facility affords one the opportunity to perform heavy-ion irradiations and electron microscopy in one instrument, thus allowing studies of (a) the formation of vacancy loops from displacement cascades at low temperature and (b) the development of defect damage as a function of ion dose and as the sample is annealed.

The response of Cu, Ni, and Fe to irradiation with 100 keV self-ions at room temperature is shown in the dark-field micrographs in Figure 1. Under these imaging conditions, the vacancy dislocation loops formed from the collapsed cascade appear as black-white lobe or black dot images; some examples are marked with an arrow. By comparing the micrographs in Figure 1, it is evident that the number of defects produced is highest in Cu and least in Fe. The defect yields are 0.60, 0.07, and 0.001 for Cu, Ni, and Fe, respectively. The difference between Fe and the other materials is greater than depicted in Figure 1, as the ion dose is much higher in Fe (6×10^{13} ions cm^{-2}) than in Cu and Ni (2×10^{11} ions cm^{-2}). At ion doses below 5×10^{12} ions cm^{-2}, displacement cascades generated by self-ion irradiations do not form visible dislocation loops in Fe, indicating that significant

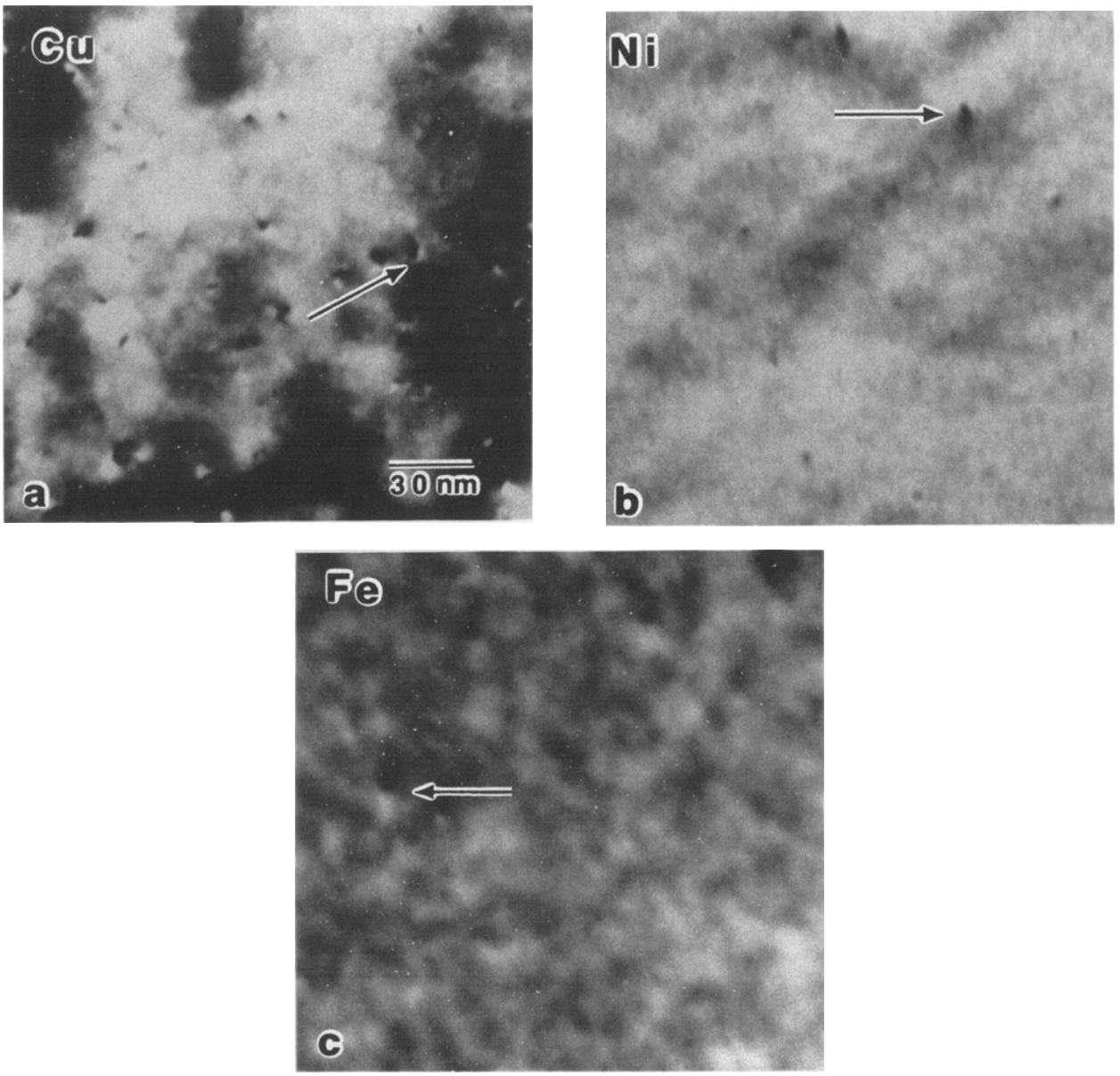

Fig. 1—Dark-field micrographs comparing the defect structure in (*a*) Cu, (*b*) Ni, and (*c*) Fe following room-temperature irradiations with 100 keV self-ions. The ion dose was in (a) and (b) 4×10^{11} ions cm^{-2} and in (c) 6×10^{13} ions cm^{-2}. In each case, the diffracting vector was 200. The arrows indicate examples of the contrast from small dislocation loops.

spatial overlap of the cascades is needed before loops are formed.[14]

Irradiation of the materials at 30 K, where vacancies and interstitials are immobile, shows that collapse occurs athermally. Except for Fe, where there is no difference between room- and low-temperature yields, the yield is generally 50 pct lower for low-temperature than for room-temperature irradiations. The occurrence of collapse at low temperature indicates high mobility of the point defects in the cascade core region during the cascade lifetime. The lower collapse probability in Ni compared to Cu is consistent with recent computer simulation results[9] and may be attributed to the shorter lifetime of the thermal spike phase in Ni. Although the recent computer simulations have not been performed in iron, the low collapse probability in Fe may also be explained in terms of the lifetime of the thermal spike.

The development of the dislocation loop population as a function of the ion dose was previously extrapolated from numerous samples irradiated to different ion doses.[18,19] These experiments[18,19] were performed at room temperature where interstitials and, in some cases, vacancies are mobile. In addition, this type of experiment suffers from the drawback that a large number of samples have to be irradiated, which assumes that the accelerator and sample conditions remain constant. Performing the heavy-ion irradiations and microstructural characterization in one instrument eliminates these problems and provides, from one sample, direct insight into the evolution of the defect microstructure.

The variation of the defect density as a function of ion dose for Cu, Ni, and Fe following a room-temperature irradiation with 100 keV self-ions is shown in Figure 2. All the data points for each material were obtained from

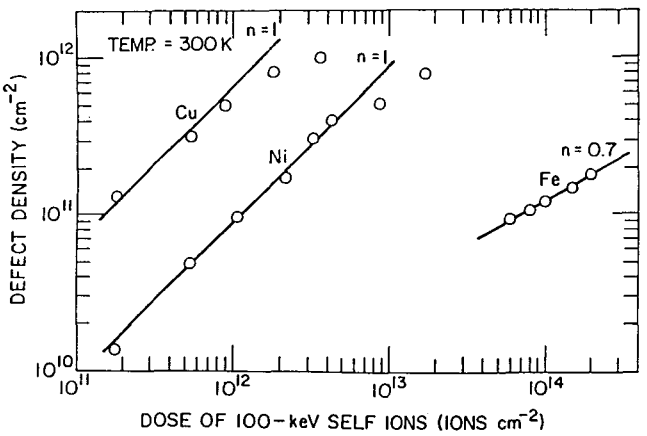

Fig. 2—The defect density as a function of ion dose for Cu, Ni, and Fe following irradiation at room temperature with 100 keV self-ions.[15]

one sample and, in many cases, from a single area. Variations in the defect density, as determined from different irradiations of the same material, were not statistically significant. The plots reveal that at low ion doses, the increase in the defect density with ion dose in linear (slope, $n = 1$); that is, the yield (the defect production rate) is initially constant. At higher ion doses, the yield changes, decreasing from its earlier value. Thus, it appears that as the ion dose increases, the probability for forming a loop from a displacement cascade decreases. The actual ion dose at which this change occurs is dependent on irradiation and material parameters. This type of response occurs in all materials (Fe, Cu, Ni, Ni 1 to 6 at. pct Al, and Ni 1 at. pct Si) that have been investigated by our group. This apparent reduction in the cascade collapse probability with increasing ion dose can be understood by examining the micrographs presented in Figure 3. These micrographs show the same area of an Ni-1 at. pct Si sample following an irradiation with 50 keV Kr^+ ions to a total ion dose of 9.9×10^{11} ions cm^{-2} in Figure 3(a) and 12.8×10^{11} ions cm^{-2} in Figure 3(b). The arrows on the micrographs indicate examples of defects that are present at the lower dose but are missing at the higher dose.

One possible explanation for the loss of loops is that they slip out of the foil. Occasionally, loops were observed to glide out of the foil; the process appeared to be enhanced by the presence of the electron beam. Alternatively, the loss of loops may be due to an incoming ion directly impacting on an existing loop. If the computer simulation models are correct, then the preexisting loop will be lost in the molten zone associated with the fresh displacement cascade. The factors governing loop collapse will again operate, and since the collapse probability is initially low, some of these fresh cascades will not form a vacancy loop. Distinction between these loop-loss mechanisms is difficult, although it should be noted that about 90 pct of the loops in the Ni systems are in the form of sessile defects. Another effect that is occasionally observed is the coalescence of defects; that is, two neighboring defects are replaced by one defect at a higher dose. Coalescence of loops can occur when the molten zone generated by an incoming ion incorporates two closely spaced loops. The loops are dissolved and their vacancies, along with those from the freshly generated displacement cascade, can combine to form a new vacancy loop. This effect provides convincing, though indirect, evidence that the cascade core is molten; such an effect would have remained undetected in more conventional irradiation experiments.

The low-temperature *in situ* irradiation experiments have shown that, in some systems, a large increase in the defect density occurs upon annealing from 30 K to room temperature. The magnitude of the increase is dependent on the material and the total ion dose. Large increases in the defect density on warm-up are observed in systems where the collapse probability is relatively low (*e.g.*, in Fe and Ni), whereas no increase is observed in systems where the collapse probability is high (*e.g.*, Cu_3Au).[17] The appearance of additional loops on warm-up is countered by the loss of some of the low-temperature loops, which have, presumably, slipped out of the foil. The loops formed during the anneal, in general, are smaller than the preexisting loops, although a small number increase in size. The size distribution for loops produced at low temperature in Ni by a 50 keV Kr^+ ion irradiation is compared with the distribution after warm-up in Figure 4. With warm-up, there is clearly a shift in the peak of the distribution to smaller sizes. Some, but not all, of this increase can be attributed to the higher instrument resolution at room temperature. As an estimate of the fraction of loops that appear because of the improved instrument resolution at room temperature, the size distribution of the warm-up loops is compared to the measured instrument resolution at low temperature (Figure 5). The size distribution shows that the size of the new loops ranges from 1.2 to 3.4 nm and that 68 pct of them lie above the low-temperature resolution limit, which for this sample was about 1.8 nm. Thus, in this case, the majority of the warm-up loops are new loops. These new loops may arise from the growth of loops that were initially submicroscopic or from uncollapsed clusters of vacancies. Diffuse X-ray scattering studies confirm that there are a number of loops/clusters with sizes below the microscope resolution limit.[20,21] In the case of iron, the additional defects start appearing at temperatures around 220 K, which corresponds to stage III.[22] The formation of additional loops during warm-up highlights the pitfall of examining at room temperature the defect structure produced by low-temperature irradiations.

B. *Case 2: Defects Produced in GaAs by Ion Implantation*

The amorphous material produced in semiconductors by ion implantation must be removed before the device can be activated. This is a particularly complex process for compound semiconductors such as GaAs. Previous electron microscopy investigations of the damage structure produced in GaAs by low-dose ($<10^{13}$ ions cm^{-2}) ion implantations suggested that amorphous zones are not produced from individual displacement cascades.[23] By using the ANL HVEM-Accelerator Facility, it has been shown that this result is incorrect and arises from a practical difficulty.

Samples of *n*-type and semi-insulating GaAs have been

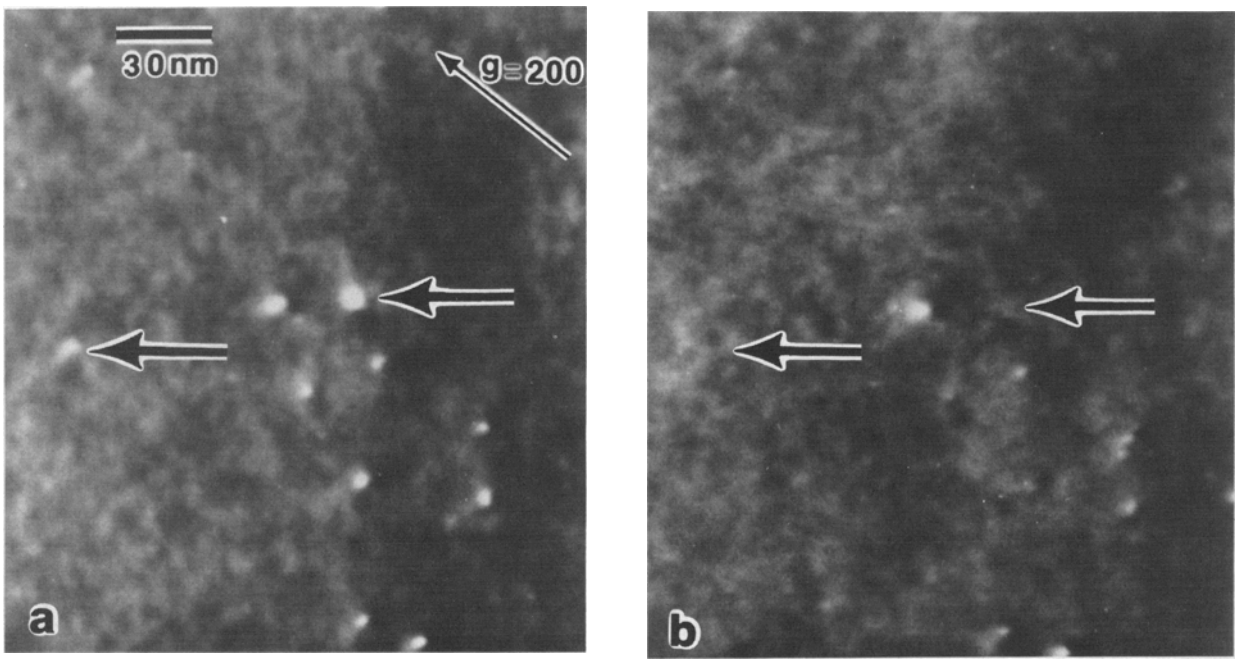

Fig. 3—Comparison of the same area in Ni-1 at. pct Si following irradiation at 30 K with 50 keV Kr^+ ions. The ion dose was 9.9×10^{11} ions cm^{-2} in (a) and 1.38×10^{12} ions cm^{-2} in (b). The arrows mark defects that are present at the lower ion dose but absent at the higher dose. The vector $\mathbf{g} = 200$.

implanted at 30 and 300 K with 50 keV Ar^+, Kr^+, and Xe^+ ions. The damage created was examined using the (220) and (400) fundamental and (200) superlattice reflections. No difference in the defect structure was detected between the *n*-type and the semi-insulating material following implantation with 50 keV Kr^+ ions at either room temperature or 30 K. Ion implantation at low temperature, where the defect mobility is limited (the Ga interstitial is thought to be mobile at 4.2 K),[24] shows that for Kr^+ ions, 95 pct of the incident ions create an amorphous zone. In contrast, when Ar^+ ions are implanted, 43 pct create an amorphous zone.

Upon warming to room temperature, it was observed that the number of amorphous zones had decreased by about 75 pct following a Kr^+ ion implant and by about 66 pct after an Ar^+ ion implant. The results of a step anneal in the *n*-type GaAs following an implantation with 50 keV Ar^+ ions at 30 K are presented in Figure 6. Qualitatively, it appears that the density of amorphous zones remains approximately constant until 250 K. Above 250 K, a large reduction in the amorphous zone density occurs. This recrystallization with increasing sample temperature is quantified in Figure 7, where the defect density is plotted as a function of annealing temperature. The defect density starts to decrease above 200 K and is reduced by more than 50 pct at 285 K. The recovery continues at room temperature with all of the zones recrystallizing within a few days. Also shown in Figure 7 is the annealing behavior of the amorphous zones created

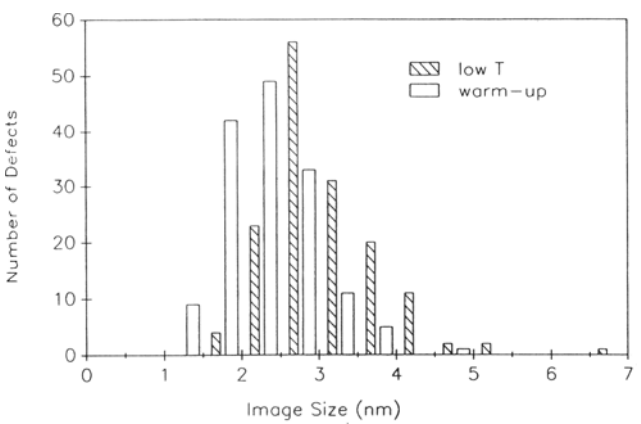

Fig. 4—Comparison of the size distribution of the defects produced in an Ni sample by a 50 keV Kr^+ ion irradiation at 30 K and after warm-up to room temperature.

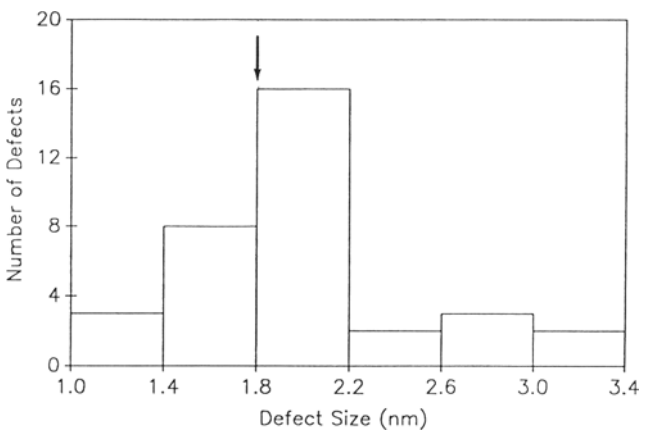

Fig. 5—Size distribution of the loops produced during warming of an Ni sample from 30 to 300 K. The arrow indicates the smallest loop diameter that was detected in the low-temperature micrographs of this sample.

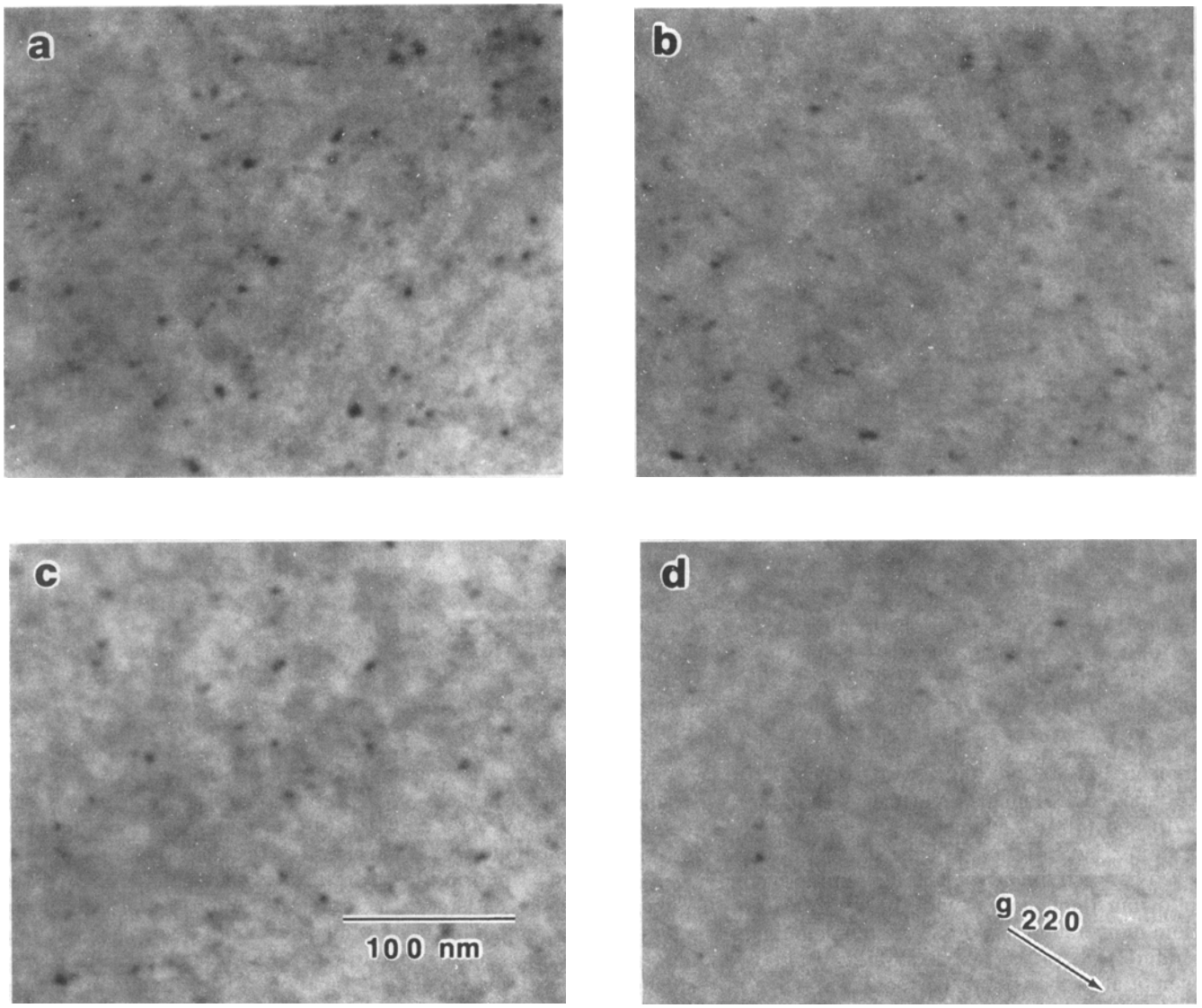

Fig. 6—Changes in the density of amorphous zones as the *n*-type GaAs is warmed from low temperature to room temperature. The sample was implanted at 30 K with 50 keV Ar^+ ions to an ion dose of 4×10^{11} ions cm^{-2}. The temperature was in (*a*) 100 K, (*b*) 200 K, (*c*) 250 K, and (*d*) 285 K.

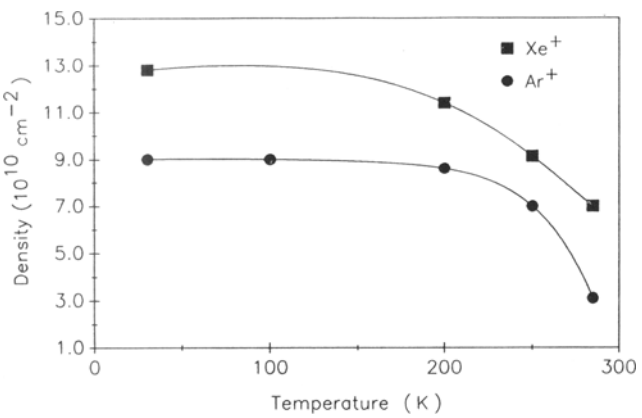

Fig. 7—Plot of the defect density against annealing temperature for GaAs implanted at 30 K with 50 keV Ar^+ (lower curve) and Xe^+ (upper curve) ions.

by a 50 keV Xe^+ ion implant. Although the initial density is higher, the same recovery trend is observed.

The instability of individual amorphous zones at room temperature explains the problem with previous experiments. Direct impact amorphization from individual displacement cascades does occur at room temperature; however, the samples need to be examined immediately after the irradiation, as the zones are unstable and recrystallize over a period of about one day.

The recrystallization rate is not dictated by the size of the amorphous zone; small zones do not recrystallize before large ones. Recrystallization of amorphous zones is dependent on the availability of the elements in the correct proportions at the interface between the damaged and undamaged material. Stoichiometric imbalances will have to be negated by diffusion from the surrounding lattice.[25] In this study, it was observed that at low

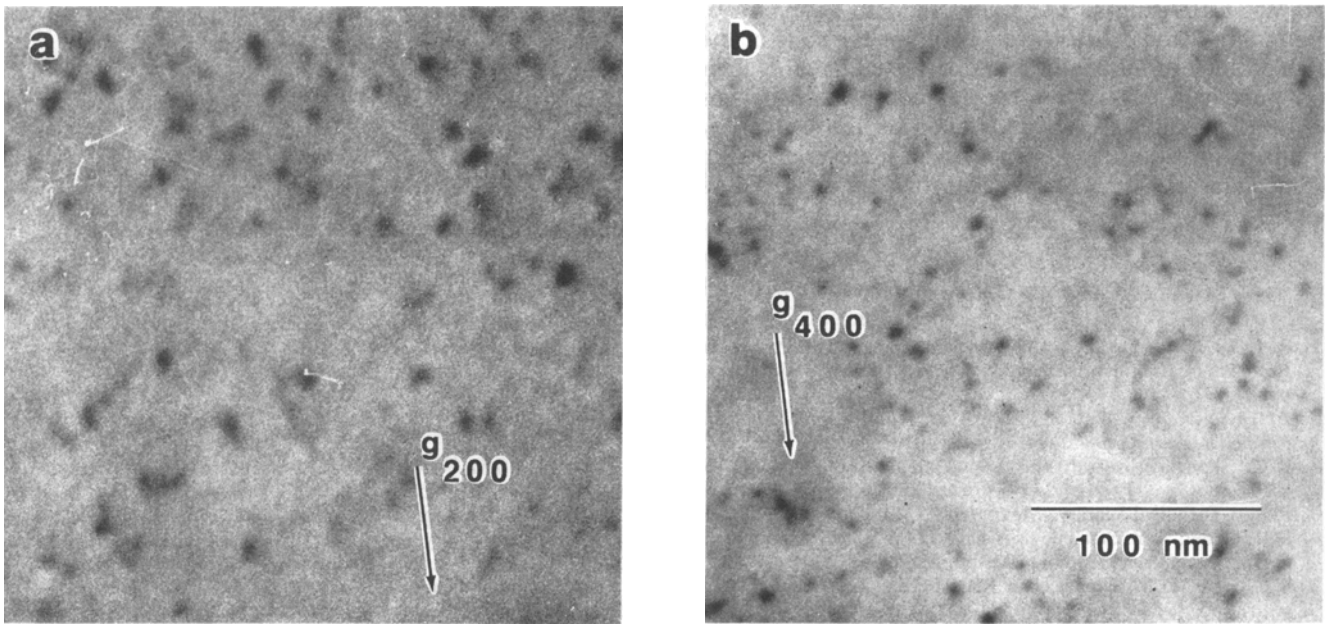

Fig. 8 — Comparison of the defect structures observed in GaAs at 30 K when the image is formed with, in (*a*), the (200) superlattice and, in (*b*), the (400) fundamental reflection. The sample was implanted at 30 K with 50 keV Kr^+ ions.

temperatures, the region of antisite disorder occupies a larger area than the amorphous zones (Figure 8). (Antisite disorder is imaged by using a superlattice reflection and the amorphous zones by using a fundamental reflection.) The difference in the area occupied by the antisite disorder and the amorphous zones is quantified in the area histogram (Figure 9). The areas of the antisite disorder zones are 50 pct larger on average than the amorphous zones. How this result affects the recrystallization rate is not well understood, but a high degree of antisite disorder may retard the kinetics of the recrystallization process. This effect is currently being investigated.

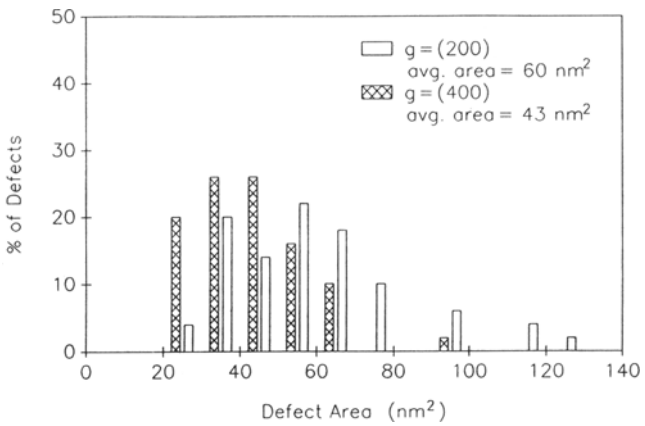

Fig. 9 — Comparison of the area distributions of the defects imaged in Fig. 8 with the (200) superlattice and the (400) fundamental reflections.

IV. SUMMARY

Through the use of the HVEM-Accelerator Facility at ANL, we have shown the following:

1. In metals, the defect production rate is constant at low ion doses but appears to decrease at higher doses. The decrease in production rate was shown to be due to the loss and coalescence of loops. Loop loss may be due to loops slipping out to the foil surface and/or by the dissolution of a loop by the direct impact of an incoming ion. Coalescence of loops may be stimulated by a fresh cascade being produced in close proximity to two previously existing loops.

   The coalescence of loops supports the notion proposed by recent molecular dynamic computer simulations that the cascade core region is molten during the thermal spike phase of the displacement cascade.
2. Vacancy dislocation loops are produced from isolated displacement cascades at temperatures where no point defects are mobile. This result can be explained by the thermal spike model.
3. Ion implantation of GaAs has shown that amorphous zones created from individual displacement cascades are unstable at temperatures above 250 K. The zone instability may be related to the degree of antisite disorder that surrounds the amorphous zones.

These effects could not have been detected by conventional irradiation experiments where the irradiations and subsequent examination are performed in different instruments.

ACKNOWLEDGMENTS

This work was supported by the Department of Energy, Basic Energy Sciences–Materials Science under Contract Nos. AC02-76ER01198 (University of Illinois)

and W-31-109-Eng-38 (Argonne National Laboratory). The authors would like to acknowledge the staff of the High-Voltage Electron Microscope Facility for their continued help and support, the Center for Microanalysis of the Materials Research Laboratory at the University of Illinois for use of microscope facilities, and the Morgan Semiconductor Company for the provision of the GaAs samples.

REFERENCES

1. R. Lyles, Jr., A. Taylor, K.L. Merkle, P. Okamoto, and P. Pronko: *Proc. 9th Int. Con. on Electron Microscopy*, Toronto, 1978, vol. 1, pp. 76-77.
2. A. Taylor, C.W. Allen, and E.A. Ryan: *Nucl. Instr. Methods in Physics Research*, 1987, vol. B24/25, pp. 598-602.
3. K.C. Thompson-Russell and J.W. Edington: *Electron Microscope Specimen Preparation Techniques in Materials Science*, Philips Technical Library, Monograph 5, Eindhoven, 1977.
4. D.K. Saldin, A.Y. Stathopoulos, and M.J. Whelan: *Philos. Trans. R. Soc. London*, 1979, vol. 292, pp. 523-37.
5. B.L. Eyre, D.M. Maher, and R.C. Perrin: *J. Phys. F*, 1977, vol. 7, pp. 1359-69 and pp. 1371-82.
6. S.M. Holmes, B.L. Eyre, C.A. English, and R.C. Perrin: *J. Phys. F*, 1979, vol. 9, pp. 2307-33.
7. H.L. Heinisch: *J. Nucl. Mater.*, 1981, vol. 103–04, pp. 1325-30.
8. T. Diaz de la Rubia, R.S. Averback, R. Benedek, and W.E. King: *Phys. Rev. Lett.*, 1987, vol. 59, pp. 1930-33.
9. T. Diaz de la Rubia, R.S. Averback, R. Benedek, and I.M. Robertson: *Proc. Workshop on Fusion Energy*, Lugano, Switzerland, 1988.
10. C.P. Flynn and R.S. Averback: *Phys. Rev.*, 1988, vol. B38, pp. 7118-21.
11. V.I. Protasov and V.G. Chudinov: *Rad. Effects*, 1982, vol. 66, pp. 1-7.
12. V.G. Kapinos and P.L. Platonov: *Rad. Effects*, 1987, vol. 103, pp. 45-57.
13. C.C. Mathai and D.J. Bacon: *J. Nucl. Mater.*: 1985, vol. 135, pp. 173-80.
14. I.M. Robertson, M.A. Kirk, and Wayne E. King: *Scripta Metall.*, 1984, vol. 18, pp. 317-20.
15. M.A. Kirk, I.M. Robertson, M.L. Jenkins, C.A. English, T.J. Black, and J.S. Vetrano: *J. Nucl. Mater.*, 1987, vol. 149, pp. 21-28.
16. K. Haga, A.C. Baily, Wayne E. King, K.L. Merkle, and M. Meshii: *7th. Int. Conf. on HVEM*, 1983, pp. 139-44.
17. T.J. Black, M.L. Jenkins, C.A. English, and M.A. Kirk: *Proc. R. Soc. London*, 1987, vol. A409, pp. 177-98.
18. K. Kitagawa, K. Yamakawa, H. Fukushima, T. Yoshie, Y. Hayashi, H. Yoshida, Y. Shimomura, and M. Kiritani: *J. Nucl. Mat.*, 1985, vols. 133 and 134, pp. 395-99.
19. H. Yoshida, Y. Hayashi, T. Maeda, K. Kitagawa, Y. Shimomura, and M. Kiritani: *Annu. Rep. Res. Reactor Inst.*, Kyoto University, 1984, vol. 17, pp. 141-45.
20. P. Erhart and R.S. Averback: Univ. of Illinois, Urbana, IL, private communication, 1988.
21. B.C. Larson, T.S. Noggle, and J.F. Barhorst: MRS Fall Meeting, Boston, 1984.
22. L. DeSchepper, J. Cornelis, G. Knuyt, J. Nihoul, and L. Stals: *Phys. Status Solidi A*, 1980, vol. 61 (a), pp. 341-48.
23. T.J. Chandler and M.L. Jenkins: *Micr. of Semiconductor Materials*, Inst. Phys. Conf. Ser., 1983, vol. 67, pp. 297-302.
24. D. Pons and J. Bourgoin: *J. Phys. C*, 1985, vol. 18, pp. 3839-71.
25. V.S. Speriosu, B.M. Paine, M.-A. Nicolet, and H.L. Glass: *Appl. Phys. Lett.*, 1982, vol. 40, pp. 604-06.